Research Signpost
37/661 (2), Fort P.O.
Trivandrum-695 023
Kerala, India

Recent Developments in Wear Prevention, Friction and Lubrication, 2010: 227-262
ISBN: 978-81-308-0377-7 Editor: George K. Nikas

# 6. Transient phenomena in elastohydrodynamic lubrication

Romeo P. Glovnea
*School of Engineering and Design, University of Sussex, England*

**Abstract.** Tribological contacts of machine components working in the elastohydrodynamic regime always experience transient conditions due to variation of speed, load, geometry, or vibrations generated within the contacts or transmitted from the environment. Given the fact that the contacting bodies and lubricant, together with the other components of the mechanisms or machine, form a dynamic system comprising of springs and dampers, this will respond to dissipate the instability caused by the variation of the above parameters. At the lubricating film level, this is done by constant-amplitude, or dampened oscillations of its thickness.

This chapter is a review of experimental research carried out in the past decade into the non-steady state elastohydrodynamic lubrication, including transient loading, sudden variation of entrainment speed and variation of micro-geometry.

## 1. Introduction

The behaviour of elastohydrodynamically-lubricated contacts in steady-state conditions is well understood both from a theoretical and an experimental point of view. However, in real applications, *elastohydrodynamic* (*EHD*) contacts rarely experience perfect, steady-state conditions, and are instead subjected to transitory variations of load, geometry or velocity of the contacting surfaces. Often more than one of these parameters varies at the same time, making the prediction of the film thickness a very difficult task, even if those variations are known, which is not usually the case. For example in gear and cam mechanisms, all these parameters vary during a working cycle, while in rolling element bearings the load changes when the rolling element enters the loading zone. The bearings from stepper motors are subjected to sudden variations of speed in a repetitive, start/stop succession. Rolling elements bearings are inherently subjected to vibrations caused by dynamic unbalances of the shaft they support, surface irregularities or simply transmitted from the surrounding. As well as these examples, all EHD lubricated

Correspondence/Reprint request: Dr. Romeo P. Glovnea, School of Engineering and Design, University of Sussex, England

contacts experience transient conditions during start and stop of the machinery of which they are part.

Steady state elastohydrodynamic films can be easily achieved in laboratory conditions, where working parameters (load, velocity, geometry, temperature) are kept constant, and the contact can be isolated from surrounding vibrations. Steady state conditions give an estimate of the effect of lubricant composition and properties upon film thickness and friction force in the contact, which are mainly used in two ways: one is to validate the theoretical models of the behaviour of EHD films, and the second is to extend or generalise results obtained in idealised conditions to practical situations. Controlled variation of one of the working parameters mentioned above allows the evaluation of its effect upon the EHD film formation under imposed transient conditions.

In recent years transient phenomena in elastohydrodynamic lubrication have received particular attention from both a theoretical and experimental point of view. A literature review of the experimental work regarding transient EHD carried out until the mid-1990s can be found in [1].

In this chapter, experimental contributions to the understanding of transient phenomena will be reviewed, with the focus on those published over the past decade. It must be mentioned that significant work and progress has also been made on the numerical simulation of the behaviour of elastohydrodynamic films in transient conditions. In fact theoretical and numerical approaches have often preceded experimental findings. It is not the intention of this review to cover the vast literature concerning numerical/transient EHD lubrication however some references will be made when the numerical work was performed to validate certain experimental results.

Transient events in elastohydrodynamic lubrication can be grouped into three main categories:

- variation of load, including impact loading;
- variation of contacting surfaces geometry, including surface roughness;
- variation of surface velocity, including squeeze, entrainment, and a combination of the two.

# 2. Background

## 2.1. Mechanisms of elastohydrodynamic lubrication

Many machine elements and mechanisms transmit relative motion and forces between surfaces which make theoretical contact in a point or along a line. In

practice the contact takes place on a very small surface, which makes the contact pressure considerably large, even at relatively low loads. Assuming elastic bodies in contact, which is often the case with steel components, under typical loads, the deflection of these surfaces is predicted by the Hertz theory of elastic contact [2]. The elastic deflection of the contacting surfaces is one of the three important phenomena which are involved in the elastohydrodynamic lubrication. Another is the hydrodynamic effect, which is responsible for the "lift" or load carrying capacity of the bearing and it is described by the Reynolds equation [3].

$$\frac{dp}{dx} = 6U\eta\left(\frac{h-h_c}{h^3}\right) \tag{1}$$

Where $p$ is the pressure, $U$ is the average velocity of the surfaces in direction $x$ of the flow, $h$ is the current film thickness and $h_c$ is the film at the position where pressure is maximum. The third mechanism required is the variation of the fluid's viscosity with pressure. Putting these three phenomena together in an analysis of an exquisite simplicity and elegance, Grubin and Vinogradova were able to reveal the mechanisms of elastohydrodynamic lubrication [4] of linear contacts (this is also attributed to Ertel [5]). They considered that the film is completely flat and that the shape of the deformed surfaces in the inlet of the contact is given by the Hertz theory. It follows that the separation between the surfaces in the convergent inlet is the sum of the constant lubricant film thickness and the Hertzian elastic deformation ($h_s$), as seen in Fig. 1.

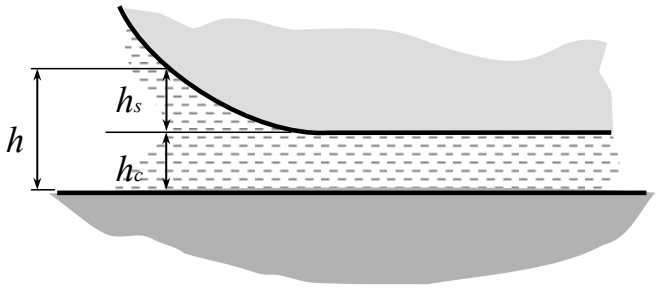


**Figure 1.** The geometry of the EHD contact inlet.

Assuming an exponential law for the dependence of the viscosity on the pressure and that the pressure remains Hertzian inside the contact, the Reynolds equation can be integrated to give, after some manipulations, the thickness of the EHD film.

$$h_c = 1.93(\alpha\eta_0 U)^{3/4} R^{3/8} W^{-1/8} E'^{1/8} \quad (2)$$

In this relation, $R$ is the reduced radius of curvature in the direction of flow ($R = [(1/R_1) + (1/R_2)]^{-1}$), $W$ is the load per unit length of contact and $E'$ is the reduced elastic modulus of the materials ($E' = [(1 - n_1^2)/E_1 + (1 - n_2^2)/E_2]^{-1}/2$).

Although approximate, Grubin's solution gives an insight into the physics of the elastohydrodynamic lubrication and has been fully supported by exact numerical solutions [6]. The latter have also revealed that the film is not completely flat inside the contact, but shows constrictions at the exit and toward the sides of the contact. Experimental evidence supported these findings [7], as illustrated in Fig. 2 for a point contact.

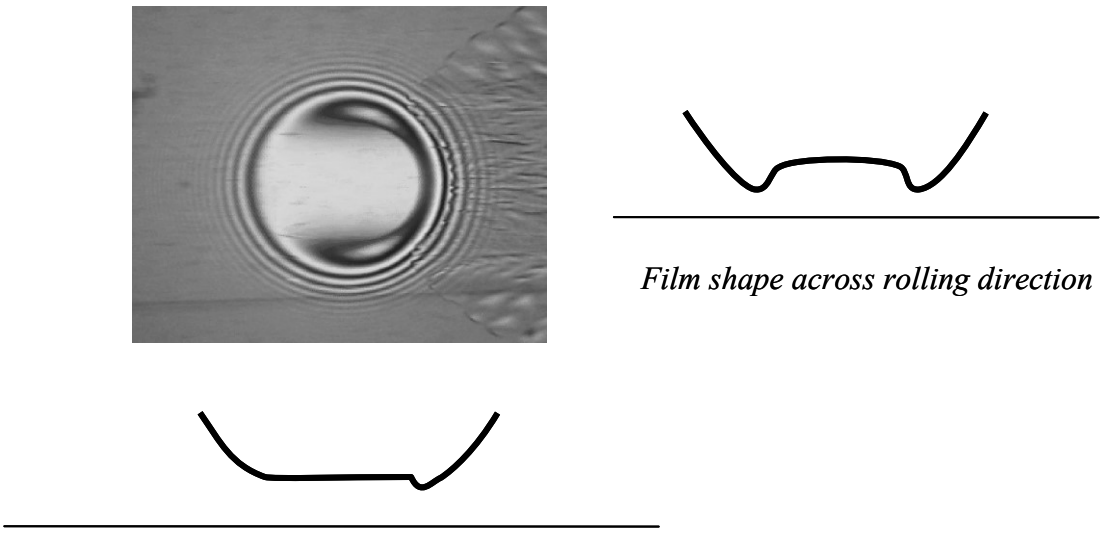


**Figure 2.** Film shape in a point contact obtained by optical interferometry.

## 2.2. EHD film thickness measurement methods

### 2.2.1. Electrical methods

Historically, electrical methods (resistive and capacitive), have preceded optical methods for studying film formation in elastohydrodynamic contacts. Usually the electrical circuit measures both resistance and capacitance, the former being used to detect full film conditions (complete separation between the contacting bodies) and the latter to measure the thickness of film, e.g. Crook [8], Archard and Kirk [9] and MacCarthy *et al.* [10]. The electrical resistance method was also used

relatively extensively for the study of mixed lubrication regime (Furey [11], Tallian *et al.* [12] Guanteng *et al.* [13]). The main advantage of electric methods is that the elastohydrodynamic contact can be formed between two bodies made out of steel, i.e. similar to the contacts found in most machine components that operate in the elastohydrodynamic regime. There are, however, some considerable disadvantages to the electrical methods. The capacitance of the contact depends of the shape of the bodies, which can only be presumed inside the contact, where large local deformations occur. The electrical methods also require knowledge of the permittivity and resistivity of the lubricant, whose variation with pressure is not precisely known. Additionally these methods only give average values over the contact area and offer no indication of the local shape of the film.

### 2.2.2. Interference of light

Many phenomena specific to light, reflection, refraction, interference, etc., can be satisfactory explained by the classical wave theory. Some of these phenomena make light a versatile tool for experimental research in a wide range of fields. In this paragraph some terms and concepts characteristic to physical optics will be briefly defined. A light wave can be represented by a sine or cosine function, as in equation (3).

$$y = A\sin\frac{2\pi}{\lambda}(x - \mathrm{v}t) \tag{3}$$

This is the equation of a transverse wave, which moves at velocity 'v' in direction $+x$, [14]. '$A$' is the amplitude and '$\lambda$' the wavelength of the light, as seen in Fig. 3.

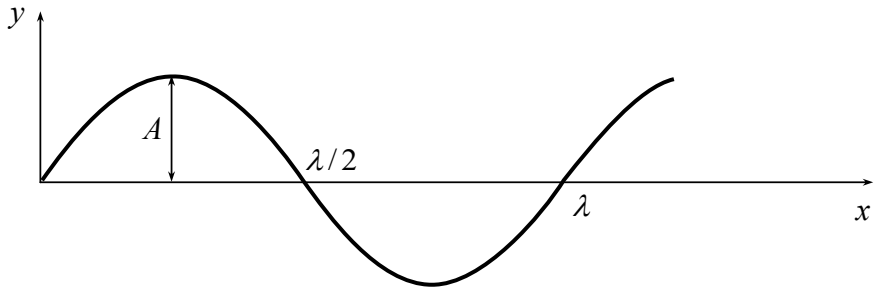


**Figure 3.** A transversal sine wave expressed by equation (3) at $t = 0$.

It is convenient to express the equation of simple harmonic waves in terms of the angular frequency $\omega$.

$$y = A\sin\left(\omega t - \frac{2\pi}{\lambda}x\right) \tag{4}$$

The quantity in the parentheses in equation (3) is known as *phase* and expresses the position of the wave at a certain time $t$. In practical terms what is important is the phase difference ($\delta$) between two beams of light when they reach a certain point.

$$\delta = \frac{2\pi}{\lambda}\Delta \tag{5}$$

where $\Delta$ is the path difference. When travelling through different media the velocity of the light waves is altered according to the refractive indexes of the media. The *optical path* is therefore defined as the product between the geometrical path and the refractive index of the medium. It follows that the phase difference can be written as:

$$\text{Phase difference } \delta = \frac{2\pi}{\lambda} \times \text{optical path difference} = \frac{2\pi}{\lambda}\Delta \tag{6}$$

Whenever a beam of light travelling through a medium with a certain refractive index arrives at the boundary with another medium with different refractive index, it is partly *reflected* and partly transmitted (*refracted*). It is important to mention that the reflection of light at any boundary is accompanied by a phase change.

When two beams of light of equal wavelength, arrive at a certain point in space a phenomenon of superposition (combination) takes place, with the net result being a change of the amplitude and intensity of the resulted light. The modification of the intensity obtained by the superposition of two (or more) light beams is called *interference* [14]. In practice, interference can be obtained, from a single beam, by *wave front* or *amplitude division* [15]. The latter takes places when a beam of light arrives at the interface between two media, being both reflected and transmitted. As this is the phenomenon exploited in the measurement of thin elastohydrodynamic films, it will be briefly explained in the following paragraphs.

Consider a beam of light which hits a thin plate of thickness $h$, at a certain angle of incidence, $\theta$. The refractive index of the material, of which the plate is made, is

*n*. At the interface between air and the plate the beam will be partly reflected, path *ADF*, and partly transmitted, path *AB*, as seen in Fig. 4. At *C*, the beam is transmitted, path *CF'*, and reflected. This internal reflection can take place several times; a phenomenon known as multiple reflection. It should be noted that the amplitudes of the reflected rays become negligible after the second internal reflection. Moreover, for the purpose of the calculation of the path difference only the first two rays are needed.

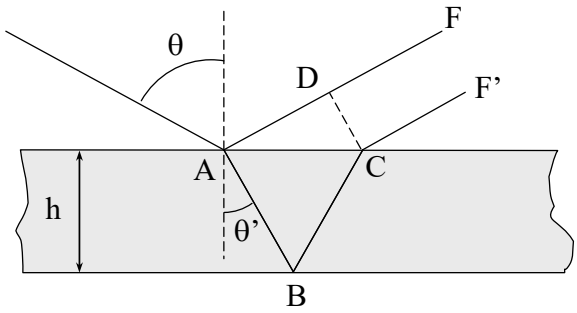


**Figure 4.** Interference by amplitude division. Calculation of path difference.

As seen by division of amplitude, the initial ray results in two rays: *AF* and *CF'*. There is a phase difference between these two rays resulting from the path difference between them and from the advance in phase produced by the reflection at *A*. The latter is equal to $\lambda/2$, for air-glass reflection. The former is the difference between the path *ABC*, travelled by the transmitted ray, in the medium with index of refraction *n* and the path *AD* travelled, in air, by the reflected ray. *D* is the foot of the perpendicular from *C* to the reflected beam.

$$\Delta = 2nAB - AD + \frac{\lambda}{2} \tag{7}$$

Distances *AB* and *AD* are found from simple geometrical considerations.

$$AB = \frac{h}{\cos\theta'} \qquad AD = AC\sin\theta = 2h\,\sin\theta\,\tan\theta'$$

The path difference becomes:

$$\Delta = 2nh\cos\theta' + \frac{\lambda}{2} \tag{8}$$

The intensity of the light at a point on the surface of the plate is given, up to a constant, by:

$$I \approx \cos^2 \frac{\delta}{2} \tag{9}$$

Replacing the phase difference according to expression (6) the intensity becomes:

$$I \approx \cos^2 \frac{\pi \Delta}{\lambda} = \cos^2 \left[ \pi \left( \frac{2nh}{\lambda} \cos\theta' + \frac{1}{2} \right) \right]$$

It is obvious that what an observer will see are bright and dark fringes. Assuming the refractive index of the medium constant, the path difference depends only on the thickness of the plate. The condition to obtain a bright fringe is given by:

$$\frac{2nh}{\lambda} \cos\theta' + \frac{1}{2} = N \tag{10}$$

where $N = 0, 1, 2, \ldots$ is the fringe order. A dark fringe is obtained for

$$\frac{2nh}{\lambda} \cos\theta' = N \tag{11}$$

For normal incidence, $cos\theta' = 1$, and a dark fringe corresponds to a thickness $h = N\lambda / 2n$. Whenever we pass from a dark fringe to another, the thickness of the plate changes by $\lambda / 2n$.

### 2.2.3. Dispersion of light; spectrometry

It was shown above that a beam of light is partly reflected and partly refracted at the separation boundary between two media with different refractive index. The refraction of white light is also accompanied by a separation into its component wavelengths [14], phenomenon known as *dispersion* and due to the variation of the refraction index with wavelength. Dispersion of light was discovered by Newton in 1665, when he passed a beam of light from the sun through a glass prism. The phenomenon is illustrated in Fig. 5.

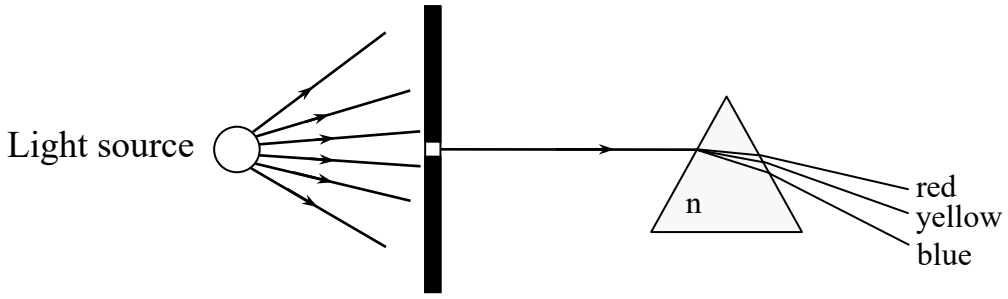


**Figure 5.** Dispersion of light through a prism.

The phenomenon of dispersion of light in its wavelength components is exploited in *spectrometers*, instruments which measure the relative amount of radiation of each wavelength. Dispersion of light in a spectrometer can be achieved by refraction in a prism or by interference by wave front division. This kind of interference is obtained passing the light through slits positioned at regular intervals, as is simply illustrated by the well-known Young's experiment, schematically seen in Fig. 6.

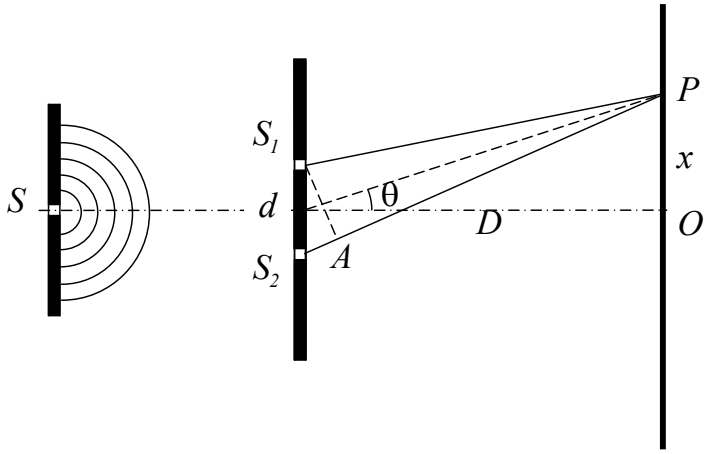


**Figure 6.** Interference by wave front division. Determination of the path difference.

When arriving at the pinholes (or slits) the wave front generated at $S$ will extend beyond the regions directly exposed to the oncoming wave, phenomenon known as *diffraction*. Assuming that the waves have the same phase at $S_1$ and $S_2$ at a certain point $P$ on a plane situated at distance $D$ they will superimpose, the intensity of the resulted wave depending on the phase difference between them, according to equation (9). The phase difference depends on the optical path difference, which approximating the sinus with its argument, can be written as:

$$\Delta = d \sin\theta = d \frac{x}{D}$$

Substituted into equation (6) the phase difference can be obtained.

$$\delta = \frac{2\pi}{\lambda} \Delta = \frac{2\pi}{\lambda} \frac{xd}{D} \tag{12}$$

Replacing this phase difference into equation (9) it can be seen that the intensity has a maximum whenever the path difference is an integral multiple of $\lambda$. Consequently we have:

$$\frac{xd}{D} = 0,\ \lambda,\ 2\lambda,\ 3\lambda,\ldots = N\lambda$$

With other words, the position of bright fringes is given by:

$$x = N\lambda \frac{D}{d} \tag{13}$$

The intensity is minima, i.e. zero, when $\delta = \pi, 3\pi, 5\pi,\ldots$ Introducing this result in (12) the condition for a dark fringe occurrence becomes:

$$\frac{xd}{D} = \frac{\lambda}{2}, \frac{3\lambda}{2}, \frac{5\lambda}{2},\ldots = \left(N + \frac{1}{2}\right)\lambda \Rightarrow x = \left(N + \frac{1}{2}\right)\frac{D}{d}\lambda \tag{14}$$

$N$ is the fringe order, as in the previous paragraph.

In spectrometers the dispersion of light is obtained with *diffraction gratings*, which are optical elements equivalent in action to a number of parallel, equidistant slits (14). It is beyond the purpose of this chapter to enter into details of the construction and theory of ruled diffraction gratings however, it can be mentioned that usually they consist of equally spaced parallel grooves, formed on a reflective coating and deposited on a substrate. Fig. 7 shows the spectra obtained by a diffraction grating. For purpose of clarity only the negative orders are shown.

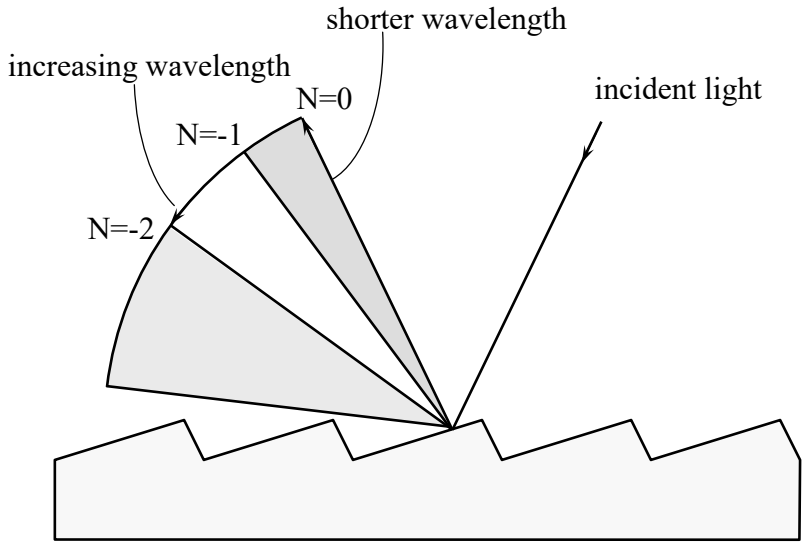


**Figure 7.** Dispersion of light by a diffraction grating.

### 2.2.4. EHD film thickness measurement by optical interferometry

For research purposes, electrical methods of measuring film thickness in EHD contacts have gradually lost ground in the favour of the optical interferometry technique, which eliminates most of the disadvantages mentioned before and allows the mapping of the whole contact with a sub-micron resolution (Cameron and Gohar [7], Foord *et al.* [16]). Developed in the early sixties, this method employs a flat, transparent disc (usually glass or sapphire), loaded against a shiny steel ball or roller. The contacting flat surface is coated with a semi-reflective metallic layer (chromium) such that any incident light shone onto the contact (usually monochromatic), is twice reflected, firstly at the glass-metal layer interface and secondly at the ball/roller surface as seen in Fig. 8.

Upon recombination the path difference between the reflected rays results in either constructive or destructive interference. The main limitation of the method in this form is that it cannot distinguish between films thinner than approximately a quarter of the wavelength of the light used.

The refinement that overcame this limitation was the addition of a solid spacer layer on top of the semi-reflective chromium layer. Made out of silica ($SiO_2$) the spacer layer has a refractive index close to that of mineral oils, which makes it act as a ‘solid oil’, increasing the separation between the surfaces of the contact and thus allowing measurements of films theoretically of any thickness. The benefits of the spacer layer were fully exploited in ultra-thin film optical interferometry method (UTFI), which uses white light and a spectrometer to disperse it into its

component wavelengths as shown in Fig. 9. The resolution of this technique is of the order of nanometres [17, 18].

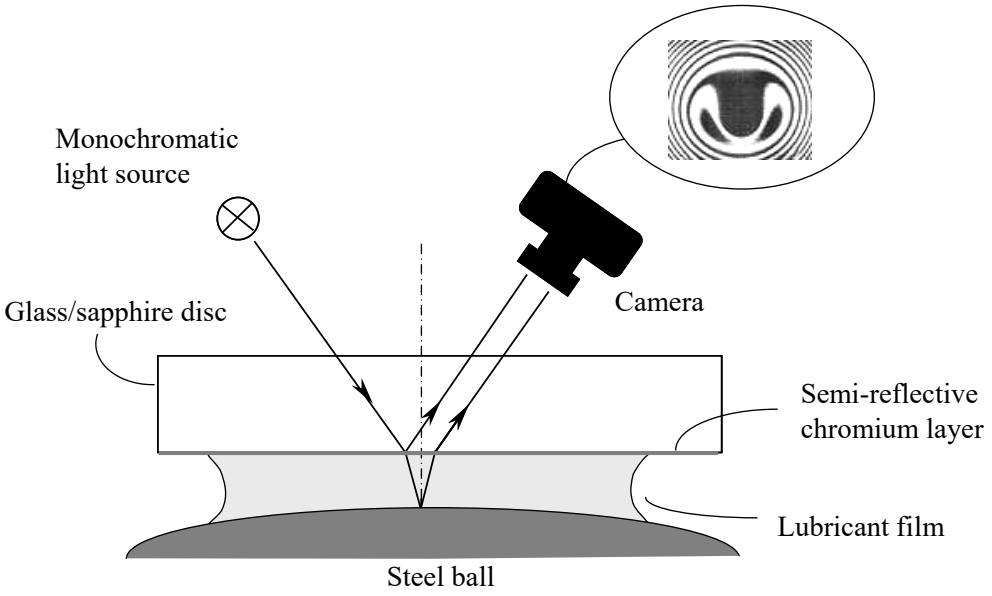


**Figure 8.** Principle of optical interferometry.

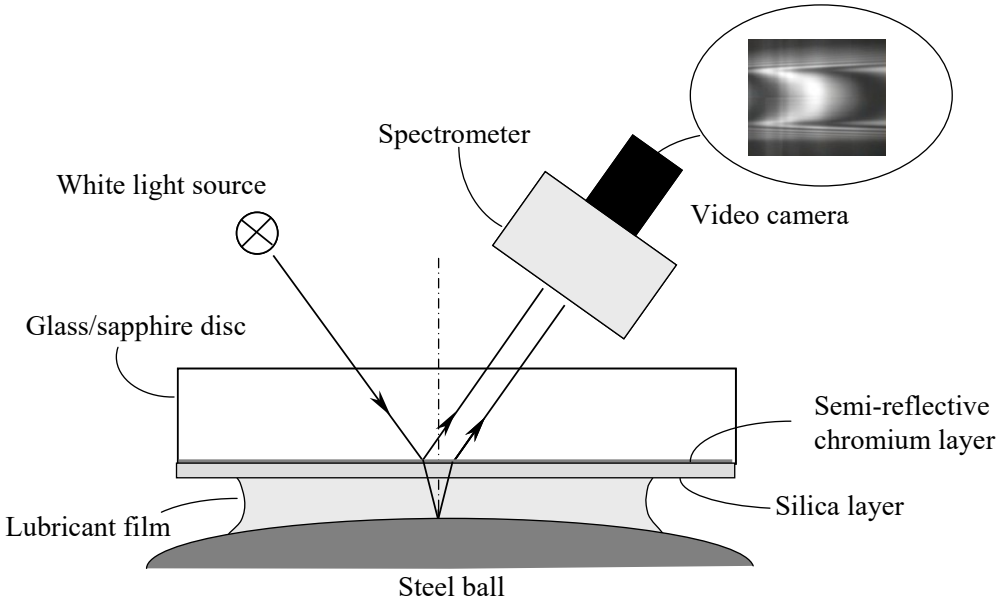


**Figure 9.** Ultrathin film interferometry technique.

## 2.3. Early experimental work on transient EHD lubrication

As electrical methods were historically first used for the study of EHD films, it is natural that they were employed in the early study of transient phenomena [19-21]. Vichard [20] carried out major theoretical and experimental studies into the effect of load variation upon EHD film thickness. He used the electrical capacitance method to measure the film thickness in the contact formed between a cam and a follower and compared with theoretical predictions. With the development of optical interferometry, and the increased attention to non-steady effects in elastohydrodynamic lubrication, this method started to be used for transient studies as well. Sanborn and Winer reported a study on the effect of transient loading upon the film thickness in pure sliding EHD contacts [22]. The interferometric fringes of the contact were recorded using high speed video during rapid change of the applied load. The researchers concluded that film thickness during rapid loading in a sliding/rolling experiment could be predicted from the steady-state behaviour; however, it should be noted the speed of load variation was limited by the acquisition speed of the camera used. Notable early experimental work on transient EHD lubrication using optical interferometry is also due to e.g. Hoglund and Jacobson [23], Ren *et al.* [24], Larson and Lundberg [25] and Sugimura *et al.* [26], among others. To be noted that while in earlier experimental work, employing electrical methods, mainly line contacts (characteristic to spur gears and cams) were studied. Although in optical interferometry both line and point contact can be obtained, it is much simpler to use a ball against a flat arrangement, in order to avoid alignment problems. It follows that all experimental work described in this chapter refers to point contacts. It is only reasonably to assume that the basic phenomena found in transient lubrication of point contacts apply in a similar fashion to line contacts.

# 3. Behaviour of EHD films in transient conditions

## 3.1. The effect of dynamic variation of load upon the behaviour of EHD films

It is known that load change has little influence on steady-state EHD film thickness. For this reason experimental studies on this aspect of non-steady EHD lubrication are less numerous than those on speed or micro-geometry; however they are not necessarily less important. Once formed, the elastohydrodynamic film is very stiff, and inside the contact the film thickness will not change instantaneously as a response to a variation of the load. The thickness of the film is

established by the conditions at the inlet, where the pressure is relatively low and the lubricant responds to external perturbations. A sudden increase of the load both increases the contact area and creates a squeeze effect in the lubricant at the periphery of the contact. When both squeeze and entrainment are present the squeeze of the lubricant will create a perturbation that subsequently travels relatively unchanged across the contact, creating pressure fluctuations that can affect the fatigue life of the contact.

Two types of non-steady phenomena will be considered in this part: transient loading and vibrations.

### 3.1.1. Transient loading

Studies in this direction have focused on the effect of transient loading upon film thickness and friction force. Any elastohydrodynamic contact can be seen as a dynamic system, consisting of springs and dampers connected together. It would be expected that any attempt to pull this system from a steady state will inevitably lead to dampened oscillations until the system reaches another equilibrium state. This has been proved to be true for a sudden change of applied load and also for rapid variation of speed, as will be shown later in this chapter.

Wijnant *et al.* [27] applied a load step of 45 N to 165 N, on a pure rolling contact and monitored the film thickness variation with optical interferometry and high speed imaging. They observed oscillations in the film thickness, which dampened after about 22 milliseconds. They performed a parallel numerical simulation of the experiments, but did not attempt a quantitative comparison of the experiment and numerical analysis. No film thickness variation is given for the experiments, but the numerical simulation indicates that the maximum amplitude of the film thickness is about 30 per cent of the initial, steady state central value. One conclusion which is clear from their experiments is that the combined damping of the system, including the EHD film, must be small. Similar results are reported by Kilali *et al.* [28] and Sakamoto *et al.* [29]. Both showed the film thickness along the central plane of the contact following a sudden variation of load, but did not capture the variation of central film thickness with time, from which the damping characteristics of the system could have been extracted. No film thickness oscillations were found by Kaneta *et al.* [30], in a pure rolling contact subjected to a sudden load pulse of about six times the initial load magnitude. However, as in previous cases, they found that a crescent shaped fluid entrapment is formed in the inlet and transported through the conjunction at the entrainment speed. The maximum value of the thickness in the entrapped region was found to increase with the loading rate. This suggests that the formation of oscillations in the film thickness is related not only to the characteristics of the

elastohydrodynamic contact itself, but also on the dynamic behaviour of the whole assembly.

In pure squeeze (i.e. no entrainment motion) the behaviour of the system is opposite, as shown by Chu *et al.* [31]. The impact load exhibits large oscillations until it stabilises at the final value, but the film thickness falls nearly continuously, with only negligible variation.

It can be therefore concluded that load fluctuations only translate into film thickness oscillations when both entrainment and squeeze are present, the latter to create film perturbations in the inlet and the former to convect these through the EHD conjunction.

### 3.1.2. Friction coefficient under transient loading

Evidence of the frictional behaviour of transient loaded contacts is given by Workel *et al.* [32, 33] and Arhstrom [34]. Both researchers used a bouncing-ball type apparatus to obtain transient loading conditions but employed different methods to measure the normal and transversal forces during impact. Workel and co-workers focussed on a traction fluid while Arhstrom employed two mineral and one polyalphaolefin, amongst other oils, in his experiments. It is difficult to directly compare these sets of results as different types of lubricants are employed, however both show a clear (albeit small), tendency of a decreasing friction coefficient with an increasing mean contact pressure. This result is consistent with those obtained in a disc machine by Evans and Johnson [35] for the same traction fluid used by Workel *et al.*, but not for a mineral oil, for which Evans and Johnson's results conversely show an increase in the traction coefficient with an increase in the mean contact pressure.

### 3.1.3. Vibrating EHD contacts

This case is probably more relevant to practical applications, as almost all machine components encounter vibrations in their working life and the way the lubricant film transmits or eventually dampens these vibrations influences the functioning of the whole assembly of which the machine component is part of. Vibrations caused by a change of the load or entrainment velocity have been reported in various studies, as shown throughout this chapter, but systematic work dedicated specifically to the effect of vibrations upon the behaviour of elastohydrodynamic contacts is sparse. Glovnea and Spikes [36] have shown that oscillations transverse to the main rolling motion create ripples through the lubricant film thickness which propagate along the instantaneous entrainment

direction, as seen in Fig. 10. The film thickness profile along the instantaneous entrainment direction is also shown.

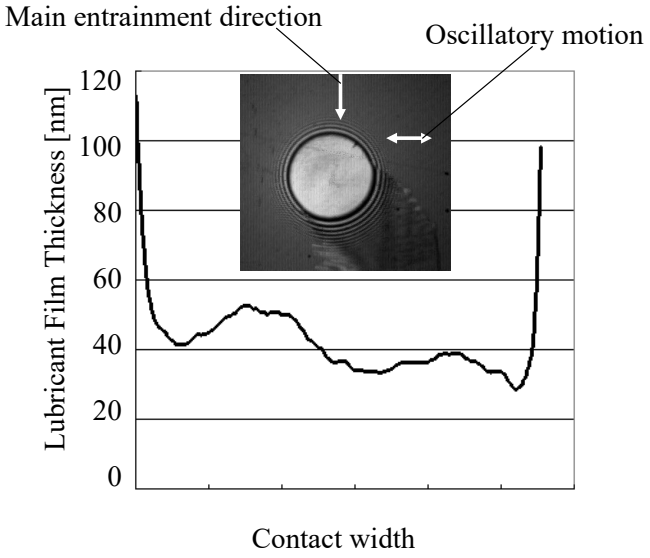


**Figure 10.** Ripples through film thickness due to lateral oscillations.

Ciulli and Bassani [37] did not induce vibrations, but instead recorded the effect of the vibrations caused by the imprecision of their instrument upon the film thickness and friction force. They found a direct correlation between load fluctuations due to the dynamics of the system and the friction force measured.

## 3.2. Effect of speed variation upon EHD film thickness

The entrainment speed enters steady-state EHD film thickness formulae with an exponent having a value of about 0.7 for line contacts [4, 6], and 0.67 for point contacts [38]. Experiments carried out for point contacts using optical interferometry have shown values between 0.6 and 0.7 which makes it one of the parameters with the strongest influence upon the film thickness [39, 40]. The EHD film's thickness is much smaller in comparison to its width or length, which makes the inertia forces due to acceleration small relative to viscous and pressure forces. Thus in most practical applications inertial forces in the lubricant film, due to the variation of entrainment speed, are negligible [41, 42]. It can hence be stated that the formation of the film is governed by entrainment and squeeze. Entrainment directly determines the passage of the lubricant through the conjunction, as it is known that once the thickness is established by the conditions at the inlet, in order to maintain the continuity of flow the lubricant travels along the contact with its

thickness unchanged. The squeeze effect occurs when one solid body drops or rebounds on a lubricated surface, or when the two solid surfaces approach or separate rapidly due to a variation of the entrainment speed.

Research into the effect of entrainment speed variation has addressed five particular types of motion:

- speed ramp (start from rest or step of entrainment speed);
- sudden stop (shut down or collapse);
- unidirectional variation of entrainment speed;
- repetitive start-stop;
- reversal of entrainment.

The steady-state EHD film thickness equations predict that, during start from rest under constant acceleration the film must exhibit a wedge-like shape until the lubricant completely separates the two surfaces. However, experimental evidence on the behaviour of the elastohydrodynamic film during starting from rest has shown that this type of behaviour is not always the obeyed. Depending on its properties and the acceleration, the lubricant either forms a wedge shaped film, or travels through the conjunction as a front of almost constant thickness until it reaches the outlet of the contact and a complete film is established over the whole contact area [43, 44].

Figures 11 and 12 compare the theoretical, steady state and measured transient film profile at certain time intervals after start of motion from rest. The entrainment speed is increased from 0 to 0.2 m/s at an average acceleration of 5 $m/s^2$ [44]. A wedge-like film was only formed for low viscosity and pressure/viscosity coefficient oils, and under low accelerations.

When a stepped front of lubricant is formed, the thickness of this step is larger than the film thickness corresponding to the entrainment speed reached at the outlet of the contact. For high viscosity and pressure/viscosity oils the ratio of the thickness of the first front to that corresponding to a steady state thickness can be as large as 3:1. As the entrainment speed increases further, a second stepped shaped front forms as soon as the first front exits the contact.

If the acceleration is sufficiently high, the time needed for the speed to reach its final value is equal to or less than the time needed for the first front to arrive at the exit of the contact. In this case the two fronts overlap and the film thickness overshoot results in a series of dampened oscillations about the thickness corresponding to the final, steady state entrainment speed, as illustrated in Fig. 13.

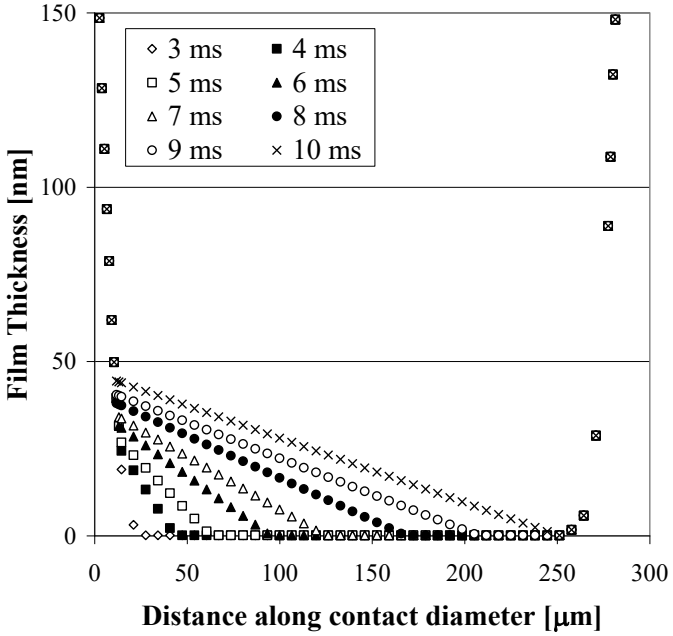


**Figure 11.** Theoretical film build-up at sudden start of motion.

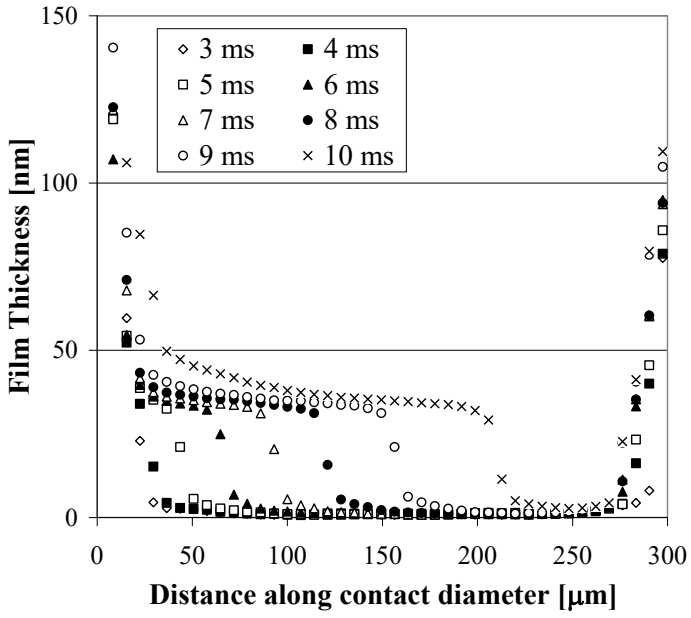


**Figure 12.** Measured film build-up at sudden start of motion.

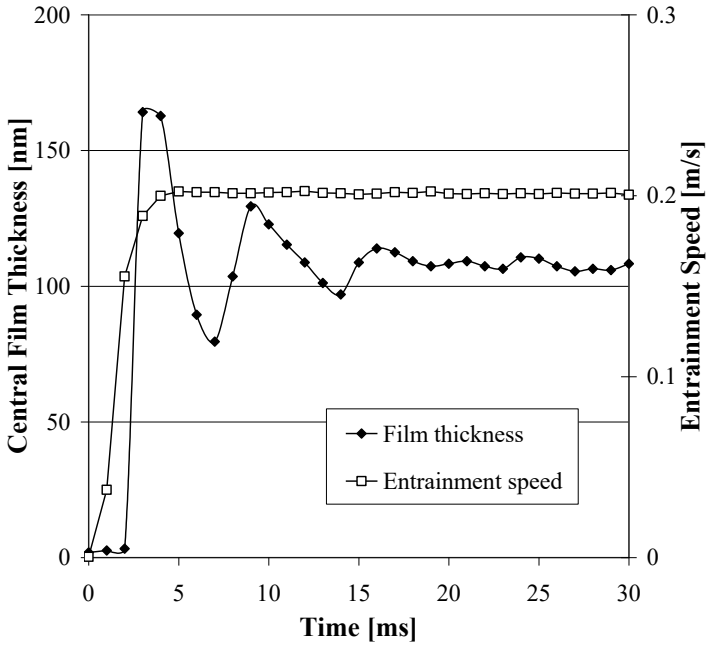


**Figure 13.** Central film thickness during sudden start of motion.

The acceleration in this case is 50 m/s$^2$, for which the time needed for the first front to travel through the contact is about 3.3 milliseconds. This is close to the theoretical time of 4 milliseconds required by the entrainment speed to achieve its final value. The variation of the entrainment speed is also seen in Fig. 13. Similar oscillations of the film thickness were observed when a sudden step was applied to the entrainment speed of a contact running at steady state conditions [45].

This behaviour is analogous to the behaviour of any system incorporating a spring and dashpot which is suddenly taken out of its steady-state condition. Numerical analysis of the dynamics of the start-up process of a similar system revealed induced oscillations in the film thickness; however those were of much smaller amplitude and larger frequency than the values measured [46]. A possible explanation given by Glovnea and Spikes [44] is based on the work of Kettleborough [47] on film thickness oscillations induced in rapidly-accelerating, hydrodynamic slider bearings. This analysis assumes a delay in the build-up of the hydrodynamic pressure due to the finite time needed for the momentum transfer across the fluid film. Of course, in the case of an elastohydrodynamic film, the situation is more complex, involving the elastic deformations of the surfaces, the transverse compliance of the solid, contacting surfaces, the squeeze effect in the film, and the dynamic behaviour of the loading system. A thorough theoretical analysis including all these factors has not been attempted.

In pure sliding tests, with a moving glass disc and a stationary ball, an intriguing phenomenon takes places, as reported by Kaneta [43]. During the film build up phase, a deep, conical-shaped dimple forms in the central area of the contact. For the particular conditions and lubricant used, the maximum film thickness was observed to be about 60 per cent larger than the final, steady state thickness. The time evolution of the central film thickness also shows dampened oscillations of the central film thickness, but of a different origin from those reported earlier [44, 45]. During the dimple formation the minimum thickness of the film was not observed at the sides of the contact (as is the case for steady state conditions), but at the contact exit. No notable dimple was formed in pure rolling or pure sliding with the ball moving and the disc stationary. Kaneta [43] concludes that the dimple is the result of solidified oil in the centre of the contact, thus slip may occur between the lubricant and the boundary surfaces. It is also worth mentioning that such dimples form more readily with oils that have a relatively low viscosity, but a large pressure/viscosity coefficient. The fact that the pressure/viscosity coefficient is the lubricant property with strongest influence upon film thickness in transient conditions supports the results obtained during sudden halting of motion, as described later.

The situation opposite to that described above is that of sudden decrease of entrainment speed under constant deceleration (sometimes referred to as “contact shutdown”). Studies of the EHD film behaviour under controlled deceleration have revealed that two distinct stages of the film behaviour can be observed. During the first stage both entrainment and squeeze are present, with the latter becoming more dominant as the film thickness decreases. In the second stage entrainment is negligible and the film collapses at the periphery of the contact entrapping the lubricant inside [48, 49].

Central and minimum film thickness variation during collapse is compared to film thickness predicted by steady state behaviour in Fig. 14, obtained for the deceleration of 200 $m/s^2$ and an initial entrainment speed of 0.5 m/s. Relative film is calculated by dividing the actual value to the initial, steady-state thickness. The figure shows that during the first stage the central film thickness is significantly larger than that predicted by the steady state theory. The origin of this enhanced film is based on two mechanisms: one is squeeze, and the other is the time lag between the film formation at the entrance and the time when the lubricant passes the centre of the contact where the thickness was measured.

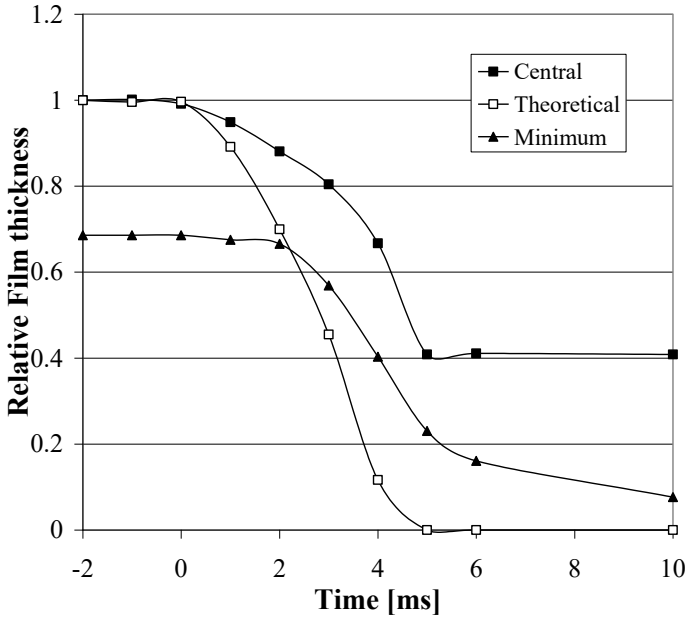


**Figure 14.** Film thickness variation during deceleration.

Sugimura *et al.* [50] deduce a simple equation for the central film thickness under acceleration, based on the continuity of flow, which takes into account the time of passage of the lubricant through the EHD conjunction.

$$h(u,a) = h_s(u)\left(1 - 0.67a\xi b/u^2\right) \tag{15}$$

In this equation, $h_s$ is the steady state film thickness, $u$ is the entrainment speed, $a$ is the acceleration, $b$ is the contact radius, and $\xi$ is a non-dimensional parameter expressing the upstream distance where the film thickness is established. This formula compared well with experimental results obtained earlier by the authors, in accelerating/decelerating tests [51], when $\xi$ took a value between 4 and 9.

A semi-analytical solution developed for film thickness during sudden halting of motion, which incorporates both entrainment and squeeze is given in [42]. This solution was based on the assumption that the inlet geometry does not change significantly during the deceleration phase, an assumption proved experimentally to be correct over about 85 per cent of the stopping time. This behaviour was also observed by Sugimura *et al.* [51]. From Reynolds' theory, the pressure gradient equation takes the form:

$$\frac{\partial p}{\partial x} = 6\eta U \frac{h - h_O}{h^3} + 12\eta \dot{h}_O \frac{x - x_O}{h^3} \tag{16}$$

This equation can be treated in a fashion similar to that used by Grubin [4] to yield, after some transformations, a central film thickness of the form:

$$h_O = h_S\left(1 - 6.522\frac{b}{h_O}\frac{\dot{h}_O}{U}\right) \tag{17}$$

This is a Bernoulli-type differential equation, which can be solved analytically to give a central film thickness expressed by the equation:

$$h_o(t) = \frac{h_s}{e^{\left(-\frac{1}{6.522\ b}\int_0^t U\,dt\right)}\left\{\frac{h_s}{h_i} + \frac{U^{8/11}}{6.522b}\int_0^t\left[U^{3/11}e^{\left(\frac{1}{6.522\ b}\int_0^t U\,dt\right)}\right]dt\right\}} \tag{18}$$

where $h_i$ is the initial film thickness, whilst the other parameters have the same meaning as in equation (1). If a power relationship between the film thickness and the entrainment velocity is assumed, equation (17) can be transformed into:

$$h_O = h_S\left(1 - 4.74b\frac{a_O}{U^2}\right) \tag{19}$$

This is exactly the same as equation (15), if $\xi$ is equal to 7.11.

The formation of fluid entrapment had been observed previously, but mainly for normal approach, where the film formation is governed by pure squeeze motion. The main difference between the two cases is that in rapid deceleration the load is practically constant, while in pure squeeze the impacting load exceeds many times the falling body's weight.

Tests carried out for a range of working parameters have shown that the central thickness of the entrapped fluid has little dependence on the initial entrainment speed. It instead depends largely on the viscosity and pressure/viscosity coefficient of the lubricant. The latter two parameters also seem closely related to the shape of the entrapment. The curves in Fig. 15 were recorded one second after the entrainment had completely ceased. For a low viscosity and pressure/viscosity coefficient lubricant the entrapment has a bell shape, indicating significant radial fluid flow both during approach and after the complete halting of motion, as indicated by profile 1 in Fig. 15. Profile 2 was obtained for a lubricant with a relatively low, atmospheric pressure, viscosity and a very large pressure/viscosity

coefficient. In this case the relatively modest viscosity ensures a quick collapse of the film at the periphery and a rapid encapsulation of the lubricant inside the contact. The large pressure/viscosity coefficient results in an effective viscosity of about 1 GPa inside the contact, according to the Barus formula. Consequently the core of the lubricant inside the contact escapes slowly, once the entrapment is formed. This combination results in a thick plug of fluid entrapped which shrinks from the edges whilst its thickness remains nearly unchanged in the centre of the contact area. The other two lubricants show consistent behaviour. Profile 3 was obtained for a large viscosity and relatively low pressure/viscosity coefficient, whilst profile 4 indicates a lubricant with large viscosity and relatively large pressure/viscosity coefficient.

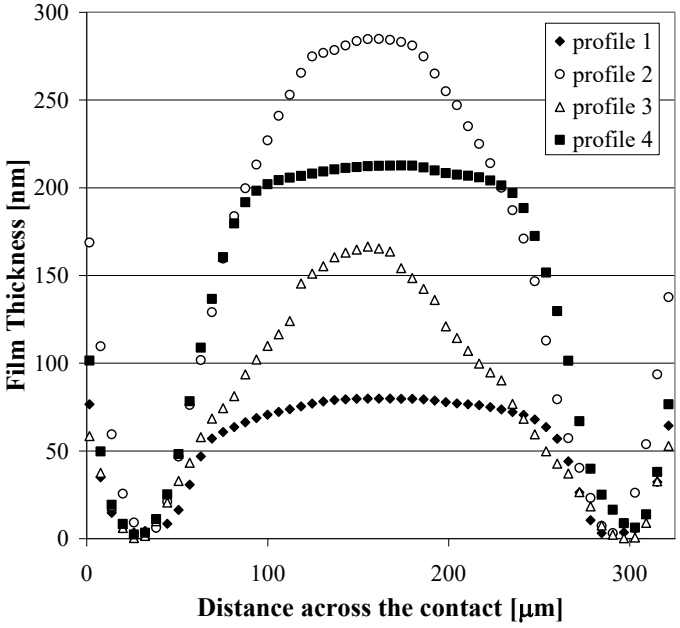


**Figure 15.** Shape of entrapped lubricant during halting of motion.

Further evidence supporting the dependence of the thickness of the entrapped film on the pressure viscosity coefficient and the viscosity of the lubricant, during sudden halting of motion, has been provided by Ohno and Yamada [52]. They have shown that the maximum thickness of the entrapped film follows a power law dependence of the product between the pressure viscosity coefficient, the viscosity and the acceleration, $(\alpha\eta a)^{0.74}$. Although these tests were carried out at relatively low accelerations of about 0.1 m/s$^2$, this relationship has been confirmed for a wider range of accelerations and lubricants as reported by Glovnea and Spikes [48].

Numerical simulations of the contact during deceleration, under the same conditions as those in [49], have been carried out and demonstrated the same qualitative behaviour and relatively good quantitative correlation with the experimental results [53, 54].

A combination of the previous cases is repetitive start/stop motion. This is governed, as explained above, by entrainment and squeeze; however the frequency of the speed variation plays an important role [51, 55, 56]. At low frequencies the film collapses partially or completely, depending on lubricant properties. At higher frequencies, the squeeze effect and entrapment formed prevent the direct contact between the bounding surfaces, which helps avoid seizure of the surfaces during rapid start under load.

Experiments with cyclical variation of the entrainment speed can be of three types: unidirectional variation (pulsating cycle), offset velocity oscillation and reversal of entrainment (alternating cycle). The time lag due to the fluid passage and the squeeze at high frequencies are the two phenomena that govern the film thickness [51, 57]. The latter will also depend on the lubricating properties of the oil, i.e. viscosity and piezo-viscosity coefficient. Figure 16 shows the ratio between measured and theoretical steady state central film thickness for two oils with similar viscosity but with the pressure/viscosity coefficient for oil 2 about 30 per cent higher than that of oil 1.

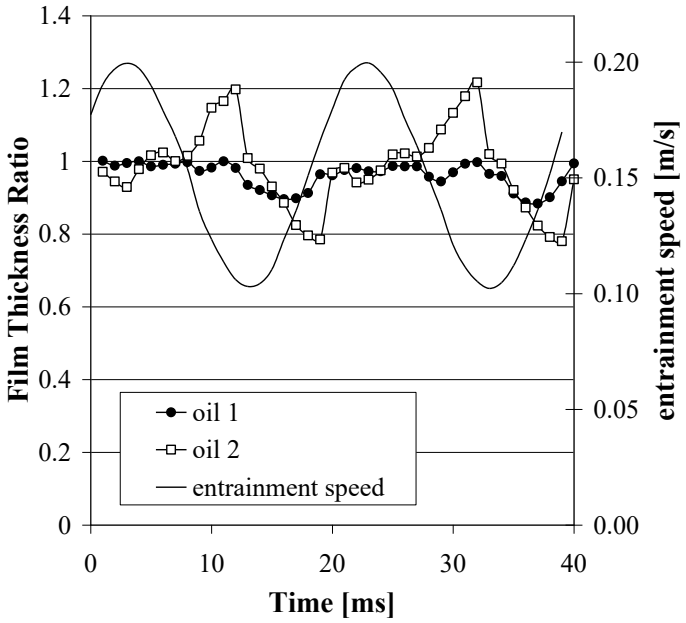


**Figure 16.** Relative central film thickness during pulsating velocity cycle.

The disc is driven at a constant velocity of 0.1 m/s while the ball's velocity varies sinusoidally between 0.1 m/s and 0.3 m/s, at 50 Hz frequency. As was observed in sudden stop tests, the oil with the larger pressure/viscosity coefficient shows a larger variation from the theoretical profile. This could be attributed to large fluctuations of the film thickness in the inlet, due to the variation of entrainment speed and squeeze. These fluctuations then travel through the contact eventually reaching the centre where the film thickness is measured.

In pulsating speed tests, the central film thickness reaches minimum values some time after the moment of zero entrainment. This delay has been shown to be proportional to the acceleration. Furthermore, unlike the entrainment speed, the central film thickness never falls to zero during the cycle of motion.

The basic behaviour observed in start/stop or pulsating motion is also found in reciprocating motion. This is because, as in the previous cases, the film thickness formation is controlled by squeeze and entrainment [58-61]. The most notable difference between reciprocating motion and unidirectional motion is that in the former case the film recovery is a slower phenomenon attributed to lubricant starvation when reversal of entrainment takes place. Based on a combined experimental and numerical study, Izumi *et al.* show that care must be taken in considering fluid replenishment after reversal when modelling reciprocating motion [60].

The combination of continuity of flow and squeeze of the film can preserve a film thick enough to completely separate the solid surfaces even if the entrainment speed falls to zero. At the same time these effects cause large variations of the film thickness, which induce significant fluctuations of the local pressure over the contact area, which will likely have a negative effect upon the fatigue life of the contact.

## 3.3. Effect of micro-geometry upon EHD film behaviour

Early measurements of film thickness in systems with varying geometry such as cams and gears were carried out using the electrical capacitance method [19, 20]. In addition to its limited precision this method also does not have the ability to map the contact thickness over its entire area. Optical methods have this ability but it is extremely difficult to implement them into a varying geometry system since, in these systems, the contact point does not remain stationary during the working cycle. This difficulty, together with the development of numerical models of EHD lubrication regime and their improved ability of simulating transient events, means there are no experimental results on the behaviour of EHD films with variable macro-geometry reported during the past two decades. Conversely the effect of

micro-geometry (roughness) on the behaviour of EHD films has been intensely studied, not only theoretically but also experimentally.

There are two approaches to the study of asperity behaviour in EHD lubrication: one is to use real, randomly rough surfaces; the other is to use artificially manufactured roughness. The advantage of the latter approach is that the shape of the un-deformed asperities is well known and a direct comparison to their behaviour inside the contact can be easily made. This helps in the understanding of asperities compression and micro-EHD film formation and enables the development of general rules which can be than applied to more complex, real-roughness systems. These asperities can be obtained by sputtering chromium on the contacting surfaces, (usually on the steel ball). Profiles of such features are shown in figures 17(a) and 17(b).

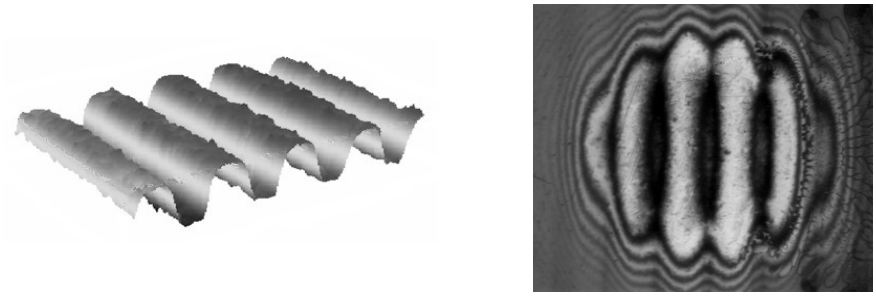

**(a)** Transversal ridges.

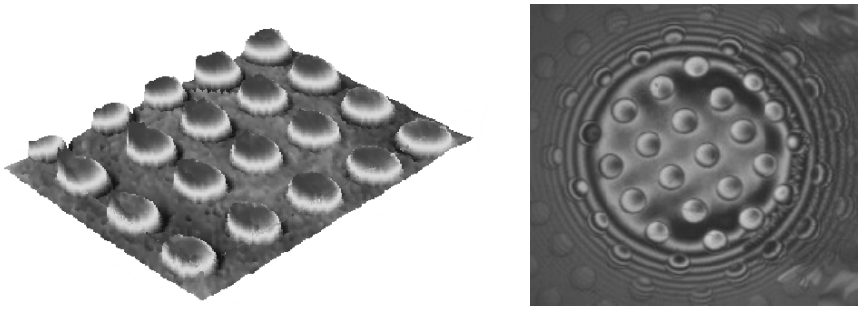

**(b)** Array of bumps.

**Figure 17.** Model roughness used in the study of mixed lubrication.

In this chapter, experimental evidence of the lubricant film thickness in contacts during the passage of simulated roughness is presented. The main types of micro-geometry features approached in various studies are:

- ridges, which can be longitudinally, transversally or obliquely oriented relative to the rolling direction [61-72];
- array of bumps [61, 64, 73-75];
- grooves (longitudinal or transversal) [76];
- single or arrays of circular dents [77-81].

### 3.3.1. Influence of asperities on local EHD film features

The existence of micro-elastohydrodynamic film at the crests of the asperities has been revealed in many studies [62, 64, etc.]. Detailed experiments by Choo *et al.* [72, 78] show that for both circular-bump asperities and transverse ridges a local "horse-shoe" shape film forms with an orientation opposing that of the macro contact. That is, the minimum film thickness is found at the trailing edge of the asperity and not at the leading edge, as is the case of the smooth, macro-EHD contact. The shape of the micro-EHD film formed by transverse ridges and circular bumps can be observed in figures 17(a) and 17(b).

Similar behaviour was observed by Kaneta *et al.* for transversely oriented ridges in pure rolling conditions [68, 71] and was attributed to the micro-squeeze action of the leading edge of the asperity, which forms a divergent conjunction just ahead of the asperity.

It can be considered that, when approaching the high-pressure region at the inlet of the contact, an asperity is compressed elastically generating at same time a perturbation of the film thickness. As the flow inside the contact is dominated by the Couette mechanism, both the compressed asperity and the film perturbation subsequently travel along the contact unchanged, at speeds that can be equal or not, depending on the slide/roll ratio. The film perturbation moves at the average speed of the surfaces, while the asperity itself moves at the speed of the surface to which it is attached. This makes the local shape of the perturbed film depend strongly on the geometry of the asperity and on the slide/roll ratio. By comparing the behaviour of the film in which the featured surface moved slower or faster than the smooth surface, Kaneta and co-workers concluded that film thickness fluctuations also depend on the wavelength of the asperities [71].

The presence of sliding makes the local shape of the film depend also on the rheology of the lubricant, as high shear rates make the lubricant shear-thin and consequently the local effective viscosity is smaller than in non-sliding conditions. Venner *et al.* [67] showed experimentally a lower asperity deformation than was theoretically predicted. This could only be explained by taking into account non-Newtonian effects.

It has also been observed experimentally that in pure rolling conditions, a dimple, or fluid entrapment forms both in front of and behind the asperities,

travelling unchanged through the contact [64, 65, 70, 72]. A similar effect has been observed by Ehret *et al.* with square shaped asperities [74] and Kaneta and Nishikawa for a single circular bump [64]. These variations in the film, in conjunction with the flattening of the asperities, give rise to large fluctuations in the local pressure, with potential implications upon the fatigue resistance of the materials. In rolling/sliding contacts these large pressure fluctuations are amplified by the fact that the film perturbation and the deformed asperity (responsible for the perturbation in the film) travel at different speeds, thus they overlap during passage through the contact.

### 3.3.2. Thickness of the micro-elastohydrodynamic film

The thickness of the film at the peak of asperities, which are rounded and not step-like, is dominated by the radius of curvature of the crest of the asperity. The ratio of the overall, central and crest film thicknesses, based on the Hamrock and Dowson equation for EHD film thickness is given by the relationship [38]:

$$\frac{h_{\text{asperity}}}{h_c} = \left[\frac{\left(R'_x\right)_{\text{asperity}}}{\left(R'_x\right)_{\text{macro}}}\right]^{1.134-X} \left[\frac{\left(1-0.61e^{-0.75\left(R'_y/R'_x\right)^{0.64}}\right)_{\text{asperity}}}{\left(1-0.61e^{-0.75\left(R'_y/R'_x\right)^{0.64}}\right)_{\text{macro}}}\right] \tag{20}$$

In this expression $X$ is an exponent, which takes a value of 0.67 in the Hamrock and Dowson equation, and varies between 0.64 and 0.67 for the two lubricants tested in [72, 73]. In the case when the asperities are sputtered on a ball $R'_{x\,\text{ball}} = R'_{y\,\text{ball}}$ and the denominator of the second square bracket becomes $\left(1-0.61e^{-0.75}\right)$. Moreover when the asperities are circular, the second bracket becomes unity and equation (20) simplifies to:

$$\frac{h_{\text{asperity}}}{h_c} = \left[\frac{\left(R'_x\right)_{\text{asperity}}}{\left(R'_x\right)_{\text{ball}}}\right]^{1.134-X} \tag{21}$$

It follows that smooth surface equations can be used to estimate film thickness at the crest of asperities as long as the latter are not step shaped.

### 3.3.3. Asperity height recovery

Theoretical studies predict that under pure rolling conditions the asperities recover their original, undeformed height completely as overall film thickness

increases [86, 87]. In other words the ratio between the deformed and undeformed height (known as 'amplitude ratio'), varies between zero (asperities completely flattened) and unity (asperities fully recovered), with the film thickness. This is supported to some extent by experimental results [66, 67, 71]. At the same time, experiments carried out over an extended range of the speed parameter have shown departures from the theoretical predicted behaviour. The first observation is that the amplitude ratio never reaches zero even in static conditions, i.e. there is not absolute conformity between the surfaces. The second is that the amplitude ratio can exceed unity, with the increase of the film thickness, to fall again at greater film thicknesses [65, 72]. The increase of the amplitude of the asperities can be explained if the behaviour of a single, transversal ridge is considered [70].

As seen in Fig 18, thicker film regions form in front of the asperity, and of lesser magnitude behind. This is as a result of the perturbation of the inlet geometry by the asperity or the formation of a fluid entrapment. Similar effects have been observed by Guanteng *et al.* [65], Kaneta [68], Felix-Quinonez [69] in transversal ridges and Felix-Quinonez for flat, square shaped asperities [75]. If the in-contact asperity height is calculated as the difference between the film thickness at the tip and that at the valley, it would result an enhanced height, as reported in [72].

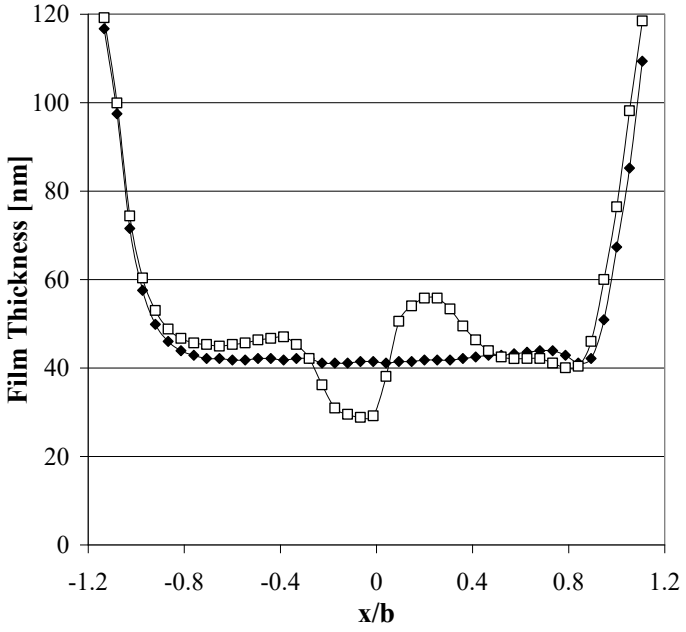


**Figure 18.** Fluid entrapment associated with a transverse ridge.

Subsequent decrease of the amplitude with the increased film thickness is more difficult to explain, but it is believed to be caused by increasing compliance of the rough surfaces due to the dynamics of the lubrication process [65, 72].

### 3.3.4. Influence of dents on local EHD film features

Whilst artificial ridges or bumps are just a tool in the understanding of the lubrication phenomena associated with real surface roughness, deliberately induced dents or groves are seen as a method of improving the tribological behaviour of lubricated machine components [77-79]. Although this method is proven in conformal contacts, it is not clear yet whether they are as effective in non-conformal, high pressure contacts. Recent experimental studies have focused on the effect of the depth of the features, pressure distribution and on the validation of numerical analyses [80-85].

Kaneta and Nishikawa [64] have observed a reduction of film thickness for a longitudinal groove, which they attribute to a reduction in the inlet pressure and to side leakage. Side leakage does not appear to occur in the case of circular dents, however depending on their depth, they distort considerably the pressure distribution and the convergence at the inlet region of the contact. Deep cavities are associated with a decrease in local film thickness while shallow ones have the opposite effect. Mourier *et al.* performed a comparative study of the behaviour of circular dents and concluded that a highly viscous oil forms inside the cavity [80]. When sliding is present, this volume of fluid is forced out of the cavity and elastically deforms the contacting surfaces.

Krupka and Hartl [82-85] show that the presence of deep, conical-shaped dents result in local film thickness reduction downstream, when the textured surface moves slower that the opposing, smooth surface. This effect diminishes with a reduction in the depth of the features and has not been observed in the case of the featured surface moving faster than the smooth surface.

Using Raman spectroscopy Vergne and Ville [81] measured the pressure distribution over a circular dent, in a pure sliding contact. They found that the presence of the dent strongly distorts the smooth-surface pressure distribution, generating pressure peaks of a magnitude twice that of the maximum Hertzian pressure.

These studies give a qualitative estimation of the behaviour of the lubricant and tendencies of the film thickness around the features, allowing future optimisation of micro-textured surfaces in elastohydrodynamic contacts.

# 4. Conclusions

Significant work, both theoretical and experimental, has been carried out during the past decade on the effect of transient conditions upon the behaviour of elastohydrodynamic films. Experimental studies have given us a better insight into the response of the lubricant film alone and lubricant-film/contacting-bodies system to variations of entrainment speed, geometry and load.

There are a series of findings which are quite clear now, regarding the behaviour of the elastohydrodynamic film in non-steady conditions.

- During pure impact loading, the dynamic load exhibits dampened oscillations, however these do not translate into oscillations of the film thickness.
- Impact loading on a steady-state contact causes fluctuations of the film thickness. These oscillations are of constant amplitude, in case of forced force fluctuations, or dampened in case of a step load.
- The film inside the contact is very stiff and does not respond instantaneously to a variation of the load. Nevertheless squeeze effect at the inlet, where the pressure is relatively low, causes perturbations of the film which subsequently travel through the EHD conjunction. It follows that impact loading only translates into film thickness fluctuations when both entrainment and squeeze are present, the latter to create film perturbations in the inlet and the former to convect these through the EHD conjunction.
- The effect of forced and free vibrations is still little studied and needs more attention in the future, in order to elucidate the effect of vibration parameters and lubricant properties upon elastohydrodynamic film behaviour.
- Sudden increase of the entrainment speed, under constant load, generates dampened oscillations of the film thickness. Currently there is no quantitative agreement between theoretical and numerical results, which invites further research into the nature of those oscillations and the effect of various parameters upon their characteristics.
- During sudden halting of motion the film collapses in two stages. In the first stage the film thickness rapidly falls, while the geometry of the conjunction shows little change. In the second stage the central film thickness stays nearly constant, while the contact closes at all sides, entrapping a plug of lubricant inside. Detailed experimental studies have revealed the effect of lubricant properties upon the thickness and the shape of the fluid entrapment.

- Analytical and semi-analytical solutions to the film behaviour under rapid deceleration, based on time of fluid passage and on a combined entrainment/squeeze effects, led to similar results.
- Experimental studies on the effect of the micro-geometry (*roughness*) of the surfaces upon the elastohydrodynamic contacts, have confirmed the existence of micro-elastohydrodynamic films. The geometry of the film, at the tip of the asperities, is a reminiscent of the macro-contact horse shoe shape, but oriented towards the trailing edge of the contact.
- It has been found that for round asperities the thickness of the micro-elastohydrodynamic film can be calculated with the relationships known for macro-contacts.
- Flattened inside the contact, the roughness recovers completely its original height as the overall film thickness increases. It has also been found that with further increase of the film, the height of the asperities inside the contact, measured from their tip to the bottom of the valleys, can exceed the initial, un-deformed height. This was explained by the formation of fluid entrapments in the valleys, due to the perturbation of the inlet geometry as an asperity approaches the high pressure zone.
- The trend of an increase of the asperity height with the overall film thickness does not continue at larger films; to the contrary, at a certain value of the speed parameter, the height of the asperities decreases. Although this behaviour has been attributed to the increasing compliance of the rough surfaces due to the dynamics of the lubrication process, more investigations are required to elucidate this phenomenon.

Regarded as a dynamic system, the lubricating film and the contacting bodies react when they are forced out of a steady state condition. They respond by generating oscillations in the film thickness, of constant amplitude in case of repetitive perturbations, or of decaying amplitude in case of singular perturbing event. From this point of view, a sudden variation of the applied load, or a step in the entrainment speed have similar effects upon the film thickness. The behaviour of the elastohydrodynamic film in transient conditions is governed by entrainment and squeeze mechanisms, which act to maintain the dynamic balance of the external load and the pressure-generated reaction.

## References

1. Larson, R. 1996. PhD Thesis, Luleå University of Technology; ISSN 0348-8373.
2. Johnson, K.L. 1985. *Contact Mechanics*. Cambridge University Press, Cambridge, UK.
3. Cameron, A. 1966. *The Principles of Lubrication*. Longmans, UK.

4. Grubin, A.N., and Vinogradova, I.E. 1949. Central Scientific Research Institute for Technology and Mechanical Engineering, Book No. 30, Moscow, 1949. D.S.I.R Trans. No. 337.
5. Cameron, A. 1985. *Tribology Int.*, **18**, 92.
6. Dowson, D., and Higginson, G.R. 1977. *Elasto-hydrodynamic Lubrication*. Pergamon, London, UK.
7. Cameron, A., and Gohar, R. (1966). *Proc. Royal Soc. London*. **A291**, 520.
8. Crook, A.W. 1958. *Phil. Trans. Royal Soc. London A*, **250**, 387.
9. Archard, J.F., and Kirk, M.T. 1960. *Phil. Trans. Royal Soc. London A*, **261**, 532.
10. McCarthy, D.M.C., Glavatskih, S.B., and Sherrington, I. 2005. *IMechE J. Engineering Tribology*, **219**, 179.
11. Furey, M.J. 1961. *ASLE Trans.*, **4**, 1.
12. Tallian, T.E., Chiu, Y.P., Huttenlocher, D.F., Kamenshine, J.A., Sibley, L.B., and Sindlinger, N.E. 1964. *ASLE Trans.*, **7**, 109.
13. Guanteng, G., Olver, A.V., and Spikes, H.A. 1999. The advancing frontier of engineering tribology, STLE/ASME, (eds: Q. Wang, J. Nethzel and F. Sadeghi), 64.
14. Jenkins, F.A., and White, H.E. 1957. *Fundamentals of Optics*. McGraw-Hill Kogakusha, LtD, Tokyo, Japan.
15. Francon, M. 1966. *Optical Interferometry*. Academic Press, New York, NY, USA.
16. Foord, C.A., Hamman, W.C., and Cameron, A. 1968. *ASLE Trans.*, **11**, 31.
17. Johnston, G.J., Wayte, R.C., and Spikes, H.A. 1991. *Tribology Trans.*, **34**, 187.
18. Glovnea, R.P., Forrest, A.K., Olver, A.V., and Spikes, H.A. 2003. *Tribology Letters*, **15**, 217.
19. MacConochie, I.O., and Cameron, A. 1960. *ASME J. Basic Eng.*, **82D**, 29.
20. Vichard, J.P., 1971. *J. Mech. Eng. Sci.*, **13**, 173.
21. Safa, M.M.A., and Gohar, R. 1986. *ASME J. Tribology*, **108**, 372.
22. Sanborn, D.M., and Winer, W.O. 1971. *ASME J. Lubrication Technology*, **93**, 262.
23. Hoglund, E., and Jacobson, B. 1986. *ASME J. Tribology*, **108**, 571.
24. Ren, N., Zhu, D., and Wen, S.Z. 1991. *Tribology International,* **24**, 225.
25. Larsson, R., and Lundberg, J. 1998. *STLE Tribology Trans.*, **41**, 489.
26. Sugimura, J., and Spikes, H.A. 1997. Elastohydrodynamics `96 (Ed. D. Dowson *et al.*), pp. 91-100 (Elsevier).
27. Wijnant, Y.H., Venner, C.H., Larsson, R., and Eriksson, P. 1999. *ASME J. Tribology*, **121**, 259.
28. El Kilali, T., Perret-Liaudet, J., and Mazuyer, D. 2004. *Proc. 30th Leeds-Lyon Symposium on Tribology* (Elsevier, ISBN: 9780444517067), 409.
29. Sakamoto, M., Nishikawa, H., and Kaneta, M. 2004. *Proc. 30th Leeds-Lyon Symposium on Tribology* (Elsevier, ISBN: 9780444517067), 391.
30. Kaneta, M., Ozaki, S., Nishikawa, H., and Guo, F. 2007, IMechE J. Engineering Tribology, 221, 271.
31. Chu, H.M, Lee, R.T., and Chiou, Y.C. 2004. *IMechE J. Engineering Tribology*, **218**, 503.
32. Workel, M.F., Dowson, D., Ehret, P., and Taylor, C.M. 2000. *IMechE J. Mechanical Engineering Science*, **214**, 309.

33. Workel, M.F., Dowson, D., Ehret, P., and Taylor, C.M. 2001. *IMechE J. Engineering Tribology*, **215**, 211.
34. Ahrstrom, B.O. 2001. *Tribology International*, **34**, 809.
35. Evans, C.R., and Johnson, K.L. 1986. *Proc. IMechE*, **200**(C5), 303.
36. Glovnea, R.P., and Spikes, H.A. 2005. World Tribology Congress III, Washington DC, USA.
37. Ciulli, E., and Bassani, R. 2006. *IMechE J. Engineering Tribology*, **220**, 319.
38. Hamrock, B.T., and Dowson, D. 1981. *Ball Bearing Lubrication: The Elastohydrodynamics of Elliptical Contacts*. J. Wiley, New York, NY, USA.
39. LaFountain, A.R., 1999. PhD thesis, University of London.
40. Glovnea, R., Olver, A.V., and Spikes, H.A. 2005. *Tribology Trans.*, **48**, 328.
41. Chang, L. 2000. *Tribology Trans.*, **43**, 116.
42. Glovnea, R.P., and Spikes, H.A. 2001. *ASME J. Tribology*, **123**, 262.
43. Kaneta, M. 1999. *Lubrication at the Frontier*. Elsevier Science B.V, p. 25.
44. Glovnea, R.P., and Spikes, H.A. 2001. *IMechE J. Engineering Tribology*, **215**, 125.
45. Glovnea, R.P., and Spikes, H.A. 2003. *Lubrication Science*, **15**-4, 311.
46. Popovici, G., Venner, C.H., and Lugt, P.M. 2004. *ASME J. Tribology*, **126**, 258.
47. Kettleborough, C. F. 1974. *J. Mech. Eng. Sci.*, **16**, 357.
48. Glovnea, R.P., and Spikes, H.A. 2000. *STLE Tribology Trans.*, **43**, 731.
49. Glovnea, R.P., and Spikes, H.A. 2001. *ASME J. Tribology*, **123**, 254.
50. Sugimura, J., Okumura, T., Yamamoto, Y., and Spikes, H.A. 1999. *Tribology International,* **32**, 117.
51. Sugimura, J., Jones, W.R. Jr., and Spikes, H.A. 1998. *ASME J. Tribology*, **120**, 442.
52. Ohno, N., and Yamada, S. 2007. *IMechE J. Engineering Tribology*, **222**, 279.
53. Zhao, J., and Sadeghi, F. 2003. *ASME J. Tribology*, **125**, 76.
54. Holmes, M.J.A., Evans, H.P., and Snidle, R.W. 2003. Tribology and Interface Engineering Series, **41**, 79.
55. Sugimura, J., 2002. *J. Jap. Soc. Trib.*, **47**, 752.
56. Glovnea, R.P., Spikes, H.A., and Jones, W.R. 2002. *J. Synthetic Lubrication* (Leaf Coppin), 191.
57. Glovnea, R.P., and Spikes, H.A. 2004. Transient Processes in Tribology (Elsevier), **43**, 401.
58. Jolkin, A., Larsson, R., and Ehret, P. 2000. *Proc. Int. Tribology Conf.*, Nagasaki, 313.
59. Glovnea, R.P., and Spikes, H.A. 2002. *Tribology Trans.*, **45**, 177.
60. Izumi, N., Tanaka, S., Ichimaru, K., and Morita, T. 2004. Transient Processes in Tribology (Elsevier), **43**, 565.
61. Wang, J., Hashimoto, T., Nishikawa, H., and Kaneta, M. 2005. *Tribology International*, **38**, 1013.
62. Guanteng, G., Cann, P.M., Spikes, H.A., and Olver, A.V. 1999. *Proc. 1998 Leeds Lyon Symposium on Tribology*, Elsevier Tribology Series 36 (Ed. D. Dowson), 175.
63. Kaneta, M., and Nishikawa, H. 1999. *Lubrication at the Frontier* (Ed.: D. Dowson *et al.*), Elsevier, 185.
64. Kaneta, M., and Nishikawa, H. 1999. *IMechE J. Engineering Tribology*, **213**, 371.
65. Guanteng, G., Cann, P.M., Olver, A.V., and Spikes, H.A. 2000. *ASME J. Tribology*, **122**, 65.

66. Venner, C.H., Kaneta, M., and Lubrecht, A.A. 2000. *Thinning Films and Tribological Interfaces* (Ed: D. Dowson *et al.*), Elsevier, 25.
67. Venner, C.H., Kaneta, M., Nishikawa, H., and Jacod, B. 2000. *Proc. Int. Tribology Conf.*, Nagasaki, Japan, 631.
68. Kaneta, M., Tani, N., and Nishikawa, H. 2003. *Tribological Research and Design for Engineering Systems*, (Ed: D. Dowson *et al.*), Elsevier, 101.
69. Felix-Quinonez, A., Ehret, P., and Summers, J.L. 2003. *ASME J. Tribology*, **125**, 275.
70. Glovnea, R.P., Choo, J.W., Olver, A.V., and Spikes, H.A. 2003. *ASME J. Tribology*, **125**, 275.
71. Kaneta, M., Nishikawa, H., and Matsuda, K. 2006. *Proc. IUTAM Symposium*, Springer Netherlands, 189.
72. Choo, J.W., Olver, A.V., and Spikes, H.A. 2007. *Tribology International*, **40**, 220.
73. Choo, J.W., Glovnea, R.P., Olver, A.V., and Spikes, H.A. 2003. *ASME J. Tribology*, **125**, 533.
74. Ehret, P., Felix-Quinonez, A., Lord, J., Larsson, R., and Marklund, O. 2001. *Proc. Int. Tribology Conf.*, Nagasaki, Japan, 478.
75. Felix-Quinonez, A., Ehret, P., and Summers, J.L. 2005. *ASME J. Tribology*, **127**, 51.
76. Yagi, K., Kyogoku, K., and Nakahara, T. 2004. *Transient Processes in Tribology* (Elsevier), **43**, 429.
77. Etsion, I., Kligerman, Y., and Halperin, G. 1999. *Tribology Trans.*, **42**, 511.
78. Wang, X., Kato, K., Adachi, K., and Aizawa, K. 2003. *Tribology International*, **36**, 189.
79. Kovalcenko, A., Ajayi, O., Erdemir, A., Fenske, G., and Etsion, I. 2005. *Tribology International*, **38**, 219.
80. Mourier, L., Mazuyer, D., Lubrecht, A.A., and Donnet, C. 2006. *Tribology International*, **39**, 1745.
81. Vergne, P., and Ville, F. 2006. *Proc. IUTAM Symp.*, Springer Netherlands, 201.
82. Krupka, I., and Hartl, M. 2006. *Tribology International*, **40**, 1100.
83. Krupka, I., and Hartl, M. 2007. *ASME J. Tribology*, **129**, 502.
84. Krupka, I., and Hartl, M. 2007. *STLE Tribology Trans.*, **50**, 488.
85. Krupka, I., Hartl, M., Urbanec, L., and Cermak, J. 2007. *IMechE J. Engineering Tribology*, **221**, 635.
86. Lubrecht, A.A., and Venner, C.H. 1999. *IMechE J. Engineering Tribology*, **213**, 397.
87. Hooke, C.J., and Venner, C.H. 2000. *IMechE J. Engineering Tribology*, **214**, 439.